

Rotating strange dwarfs and their indistinguishability from white dwarfs

Edson Otoniel,^{1,*} José D. V. Arbañil,^{2,3,†} Geanderson A. Carvalho,^{4,5,‡} and Fridolin Weber^{6,7}

¹*Instituto de Formação de Educadores, Universidade Federal do Cariri,
R. Olegário Emídio de Araujo, s/n – Aldeota, 63260-000 Brejo Santo, CE, Brazil*

²*Departamento de Ciencias, Universidad Privada del Norte,
Avenida el Sol 461 San Juan de Lurigancho, 15434 Lima, Peru*

³*Facultad de Ciencias Físicas, Universidad Nacional Mayor de San Marcos,
Avenida Venezuela s/n Cercado de Lima, 15081 Lima, Peru*

⁴*Departamento de Física, Universidade Tecnológica Federal do Paraná, Medianeira, PR, Brazil*

⁵*Programa de Pós-Graduação em Física e Astronomia,*

Universidade Tecnológica Federal do Paraná, Jardim das Américas, 82590-300, Curitiba, PR, Brazil

⁶*San Diego State University, Department of Physics, San Diego, 92182, California, USA*

⁷*University of California at San Diego, 9500 Gilman Drive, La Jolla, 92093, California, USA*

(Dated: February 6, 2026)

We investigate the structure of strange dwarfs, modeled as hybrid compact stars composed of a self bound strange quark matter core surrounded by a white dwarf like crust, within a fully relativistic framework. Static configurations are constructed by solving the Tolman–Oppenheimer–Volkoff equations, and uniformly rotating configurations are modeled within the Hartle–Thorne slow rotation expansion (to $\mathcal{O}(\Omega^2)$). We therefore interpret results at large fractional spins conservatively, and use the Kepler frequency mainly as a reference scale for comparing different masses and models. The stellar matter is described using a hybrid equation of state, in which the crust is modeled by a degenerate electron–ion system and the core by the MIT Bag Model. By comparing strange dwarfs with conventional white dwarfs across a range of rotation rates, we show that rotation inflates the radius and can reduce (in a quantifiable way) the separation between the two families in the (M, R) plane, potentially masking structural signatures associated with the presence of a quark core. Our results highlight the importance of accounting for rotational effects when interpreting mass radius measurements and other global observables in the context of searches for exotic compact objects in current and future high precision surveys.

1. INTRODUCTION

White dwarfs (WDs) are the most common final evolutionary stage of stars; in fact, about 90% of the main-sequence stars will evolve into WDs [76]. The most massive WDs have masses similar to that of the Sun and radii of about 10^3 km, which makes them extremely compact, with an average mass density of 10^6 g/cm³ [1]. They can remain stable against gravitational collapse only because the electron degeneracy pressure counteracts gravity.

The baryonic matter that composes a WD is thought to be primarily carbon and oxygen, or sometimes neon and magnesium. In addition, spectroscopy measurements show that WD atmospheres are dominated by hydrogen or helium [3]. However, according to the Bodmer–Witten hypothesis [20, 21], strange quark matter (SQM) may be the absolute ground state of matter. If the SQM is indeed absolutely stable, then neutron stars, WDs, or even planets could possess a core of strange matter. This possibility opens a new perspective on the internal structure of WDs.

Motivated by this scenario, the possibility of WDs containing a SQM core, known as strange dwarfs (SDs), was explored decades ago [4, 5]. Glendenning et al. [5] stud-

ied the stability of SDs under radial perturbations and showed that this class of objects can remain stable even when the normal matter density exceeds the neutron-drip density threshold, because the SQM core stabilizes the star. Some works revisited the stability criteria of SDs using different mathematical approaches and obtained controversial results, e.g., see [11, 12]. Furthermore, [6, 7] improved the treatment of radial oscillations in the context of the phase transition, showing that radial stability depends on the boundary conditions at the phase transition.

Despite particular differences, SDs share several macroscopic similarities with ordinary WDs. For a given radius along the mass–radius relation, the SD is slightly less massive than its WD counterpart. On the other hand, for a fixed mass along the mass–radius relation, SDs have smaller radii compared to conventional WDs; see, for instance, [13]. Recently, in [8], it is found that the tidal deformability of SDs deviated by about 8% to near 50%, depending on the composition of the baryonic crust, from the values obtained for typical WDs. This makes tidal deformability a key parameter for distinguishing SDs from WDs through gravitational-wave astronomy. In [9], seven SD candidates are proposed by comparing their measured masses and radii with mass–radius diagrams. These candidates have smaller radii than other WDs with similar masses. The masses range from 0.02 to $0.12M_\odot$, with radii between 9000 and 15000 km. This mass range is classified as that of extremely low-mass WDs [10].

*Electronic address: edson.otoniel@ufca.edu.br

†Electronic address: jose.arbanil@upn.pe

‡Electronic address: gacarvalho@utfpr.edu.br

One important question concerning SDs is their origin. Current scenarios suggest two possible formation pathways: either a strange quark star accretes normal nuclear matter onto its surface, or a conventional WD captures clusters of SQM, known as strangelets [13]. Although the formation mechanism is highly relevant, it lies beyond the scope of this work. Here, we focus exclusively on investigating the macroscopic properties of rotating SDs.

The macroscopic structure, evolution, and observable properties of WDs are influenced by rotational effects. Rotation modifies the stellar equilibrium by providing additional centrifugal support, which increases the maximum mass a WD can sustain without collapsing and alters its mass radius relation [14]. Rapid rotation also produces measurable deviations from spherical symmetry, which in turn modify the moment of inertia, gravitational quadrupole moments, and tidal responses [15, 16, 81]; key parameters for interpreting binary evolution, gravitational-wave signals, and pulsation modes.

Rotation also plays an important role in the progenitors of Type Ia supernovae, where spin-up/spin-down processes impact explosion conditions and delay times [17]. Observationally, WD rotation is inferred indirectly through rotational broadening of spectral lines, variability caused by magnetic spots, and asteroseismology; see, for example, [18]. Accurate theoretical modeling is therefore essential for correctly interpreting these observations. Thus, accounting for rotation is fundamental for realistic modeling of WDs or SDs and their potential role in astrophysics.

We organize this paper as follows. In Section 2, we present the theoretical framework adopted throughout this work, introducing the equations governing stellar equilibrium in general relativity and describing the Hartle–Thorne formalism used to model uniformly rotating compact stars within the slow-rotation approximation. This section also defines the physical assumptions and limits under which the rotational treatment remains valid. In Section 3, we construct the hybrid equation of state employed to model strange dwarfs, detailing both the description of the hadronic crust, representative of white dwarf like matter, and the strange quark matter core modeled within the MIT Bag Model. We also explain the matching conditions at the core-crust interface and discuss the role of the electrostatic layer in ensuring mechanical equilibrium between the two regions. The numerical results are presented and discussed in Section 4. In this section, we analyze the relativistic stellar structure obtained from the adopted equation of state, considering both static and uniformly rotating configurations. Particular emphasis is placed on assessing the sensitivity of the stellar properties to variations of the bag constant and on quantifying the impact of rotation on global observables such as mass, radius, and compactness, allowing for a direct comparison between strange dwarfs and conventional white dwarfs. Finally, in Section 5, we summarize the main findings of this study, discuss their physical implications within the context of compact star model-

ing, and outline the limitations of the present approach, as well as possible extensions and future directions motivated by observational and theoretical developments.

2. STELLAR EQUILIBRIUM EQUATIONS, HARTLE-THORNE EQUATIONS, AND EQUATION OF STATE

For the sake of completeness, we begin by presenting the Einstein field equations that govern a system containing matter, which, in geometric units, is given by

$$G_{\mu\nu} = 8\pi T_{\mu\nu}, \quad (1)$$

with μ, ν , etc. running from 0 to 3. $G_{\mu\nu}$ represents the Einstein tensor and $T_{\mu\nu}$ stands the energy-momentum tensor. For the fluid contained in the SD, the energy-momentum tensor is placed in the form

$$T_{\mu\nu} = (p + \rho)u_\mu u_\nu + pg_{\mu\nu}, \quad (2)$$

p and ρ represent the fluid pressure and the energy density, respectively. u_μ depicts the 4-fluid velocity which follows condition $u_\mu u^\mu = -1$.

2.1. Stellar equilibrium equations

To describe the interior static spherically symmetric spacetime, the line element takes the form:

$$ds^2 = -e^{\Phi(r)}dt^2 + e^{\Lambda(r)}dr^2 + r^2(d\theta^2 + \sin^2\theta d\phi^2), \quad (3)$$

with t, r, θ , and ϕ representing the Schwarzschild coordinates. The functions $\Phi(r)$ and $\Lambda(r)$ depend only on the radial coordinate.

By means of the non-zero equations of the Einstein field equation (1) obtained by considering the energy momentum tensor for a perfect fluid (2) and the previously defined metric (3) we find the relations:

$$m' = 4\pi r^2 \rho, \quad (4)$$

$$p' = -(\rho + p) \left(\frac{m + 4\pi r^3 p}{r^2} \right) e^\Lambda, \quad (5)$$

$$\Phi' = 2 \left(\frac{m + 4\pi r^3 p}{r^2} \right) e^\Lambda, \quad (6)$$

where

$$e^\Lambda = \left(1 - \frac{2m}{r} \right)^{-1}. \quad (7)$$

The primes (') depict the derivative with respect to the radial coordinate r , and m represents the mass contained within a radius r .

The stellar equilibrium equations, also known as the Tolman–Oppenheimer–Volkoff (TOV) equations, Eqs. (4)–(6), Ref. [23, 24], are integrated from the center $r = 0$

towards this star's surface $r = R$. The process starts considering $r = 0$

$$\begin{aligned} m(0) &= 0, & \rho(0) &= \rho_c, & p(0) &= p_c, \\ \Lambda(0) &= 0, & \text{and} & \Phi(0) &= \Phi_c, \end{aligned} \quad (8)$$

and it ends when in $r = R$

$$p(R) = 0. \quad (9)$$

At the surface of the star, the interior and the exterior line elements match smoothly; thus, at this point, the potential metrics follow the relation:

$$e^{\Phi(R)} = \frac{1}{e^{\Lambda(R)}} = 1 - \frac{2M}{R}, \quad (10)$$

with M and R being the mass and radius of the star, respectively.

2.2. Hartle-Thorne equations

The Hartle-Thorne formalism is a perturbative expansion in the stellar angular velocity, truncated at second order, and it is strictly controlled when the dimensionless rotation parameter (e.g., $\Omega^2 R^3/(GM)$) remains small. For this reason, throughout this work we use the Hartle-Thorne sequences to (i) quantify leading order rotational trends, and (ii) identify the onset of a potential observational degeneracy between SDs and WDs. When we quote fractions of the Kepler frequency, Ω/Ω_K , we employ Ω_K as a convenient normalization of the spin scale for each mass and EoS. However, configurations extremely close to mass shedding should ultimately be revisited with fully two dimensional relativistic rotating-star codes, and any statement of “indistinguishability” near $\Omega \sim \Omega_K$ should be interpreted in this conservative sense.

Following [81, 82], to investigate the effects of rotation on the structure of compact stars, we used the spacetime metric with axial symmetry:

$$ds^2 = -e^{2\nu} dt^2 + e^{2\lambda} dr^2 + e^{2\mu} d\theta^2 + e^{2\psi} (d\phi - \omega dt)^2, \quad (11)$$

with the potential metrics of the form:

$$e^{2\nu} = e^{\Phi(r)} [1 + 2h_0(r) + 2h_2(r)P_2(\cos\theta)], \quad (12)$$

$$e^{2\lambda} = e^{\Lambda(r)} \left[1 + \frac{2e^{\Lambda(r)}}{r} [m_0(r) + m_2(r)P_2(\cos\theta)] \right], \quad (13)$$

$$e^{2\mu} = r^2 [1 + 2k_2(r)P_2(\cos\theta)], \quad (14)$$

$$e^{2\psi} = r^2 \sin^2\theta [1 + 2k_2(r)P_2(\cos\theta)]. \quad (15)$$

In the line element (11), the terms $h_l(r)$, $m_l(r)$, and $k_l(r)$ correspond to the rotational perturbations of order Ω^2 , specifically the contribution of both the monopole ($l = 0$) and the quadrupole ($l = 2$); setting $k_0(r) = 0$ reflects the gauge choice adopted by Hartle [81]. $P_l(\cos\theta)$ denotes the Legendre polynomial of degree l .

Meanwhile, the angular velocity of the local inertial frame $\omega(r)$ encapsulates the frame dragging effect induced by stellar rotation, emerging as a first order contribution in the expansion with respect to the star's angular velocity Ω ; with this latter running from 0 to the Kepler frequency Ω_K [83–85], which is determined by [86]:

$$\Omega_K = \omega + \frac{\omega'}{2\psi'} + e^{\nu-\psi} \sqrt{\frac{\nu'}{\psi'} + \left(\frac{\omega' e^{\psi-\nu}}{2\psi'} \right)^2}, \quad (16)$$

with the primes indicating the partial derivative with respect to the radial coordinate. In the first order contribution specifically in the dipolar sector ($l = 1$) Hartle [81] showed that $\omega(r)$, which describes the angular velocity of local inertial frames relative to a distant observer, satisfies a second-order differential equation derived from the $t\phi$ component of Einstein's field equations given by

$$\frac{1}{r^4} \left(r^4 j(r) \frac{d\omega(r)}{dr} \right) - \frac{4}{r} \frac{dj}{dr} (\Omega - \omega(r)) = 0, \quad (17)$$

with $j(r) = e^{-(\Lambda+\Phi)/2}$. Equation (17) arises directly from the $t\phi$ component of Einstein's field equations.

For a constant rotation (Ω constant), equation (17) could be rewritten in the form:

$$\frac{1}{r^4} \left(r^4 j(r) \frac{d\bar{\omega}(r)}{dr} \right) - \frac{4}{r} \frac{dj}{dr} \bar{\omega}(r) = 0, \quad (18)$$

where the new parameter follows $\bar{\omega} \equiv \Omega - \omega$. It represents the angular velocity of the fluid measured relative to the local frame of reference.

Equation (18) is solved from the center $r = 0$ to the surface of the star $r = R$. This process begins by considering the conditions at the origin of the star:

$$\bar{\omega} = \text{Constant}, \quad \left(\frac{d\bar{\omega}}{dr} \right)_{r=0} = 0. \quad (19)$$

Outside the star ($r > R$), where $\rho = p = 0$ and $j = 1$, the next solution is obtained:

$$\bar{\omega} = \Omega - 2 \frac{J}{r^3}, \quad (20)$$

with J being the total angular momentum of the star. Due to the lack of dynamical degrees of freedom at the stellar surface, both $\bar{\omega}$ and its radial derivative $d\bar{\omega}/dr$ remain continuous at $r = R$. Consequently, at this boundary, the angular momentum J and the angular velocity Ω are given, respectively, by the following expressions:

$$J = \frac{R^4}{6} \left(\frac{d\bar{\omega}}{dr} \right)_{r=R}, \quad \Omega = \bar{\omega}(R) + \frac{2J}{R^3}. \quad (21)$$

Since there is flexibility in selecting the value of $\bar{\omega}$ at the stellar core, the resulting angular velocity Ω typically does not match a preferred target value. Thus, one rescale the function $\bar{\omega}$ as follows:

$$\bar{\omega}_{\text{new}} = \bar{\omega}_{\text{old}} \frac{\Omega_{\text{new}}}{\Omega_{\text{old}}}. \quad (22)$$

3. EQUATION OF STATE

To investigate rotating SDs, we consider a crust composed of a gas of degenerate electrons and a core of SQM. Additionally, we match the two phases at the neutron-drip point by imposing continuity of the (mechanical) fluid pressure, $p_{\text{crust}} = p_{\text{core}} = p_{\text{drip}}$, while allowing for a discontinuity in the energy density across the interface, as expected for a first order transition and as in the standard strange dwarf construction [5]. In this idealized treatment, the thin electrostatic layer that ensures global charge neutrality and prevents immediate conversion of the crust (typical thickness $\ll 1$ cm in physical units) is neglected in the macroscopic structure equations, so the interface is implemented as a sharp boundary at a single radius. We emphasize that the present matching prescription specifies the equilibrium branch of interest, but dynamical stability across a sharp interface depends on the phase conversion and boundary condition prescription (see, e.g., [6, 7, 11]). These two fluid matter equations of state are described in the following subsections.

3.1. Crust Matter Composition

In the seminal works [71, 72], Salpeter and Hamada in 1961 proposed that the composition of a WD matter is primarily made up of atomic nuclei immersed in a completely degenerate electron gas. In more recent work, Otoniel and collaborators in [73] carried out an approach where the equation of state (EoS) that describes the magnetic fluid contained in a WD is derived using updated atomic mass evaluations (see, for instance, Ref. [74, 75] and the references therein). Therefore, disregarding the magnetic field within the fluid, we consider that the pressure in SD crust is primarily due to degenerate electrons and the ionic lattice, such is assumed in the internal pressure of WDs [76]. In this way, using this formalism, we regard that the total pressure in the crust of the SD is given by:

$$p_{\text{crust}}(k_F) = p_L(Z) + \frac{1}{3\pi^2 h^3} \int_0^{k_F} \frac{k^4}{\sqrt{k^2 + m_e^2}} dk. \quad (23)$$

The first term on the right hand side of equation (23) depicts the pressure generated by the relativistic degenerate electron gas, which can be expressed as follows:

$$p_L(Z) = \frac{1}{3} C e^2 n_e^{4/3} Z^{2/3}. \quad (24)$$

The last relation stems from Coulomb interactions between ions organized in a crystalline lattice, which is commonly assumed to adopt a body centered cubic (bcc) configuration within the interiors of WDs. In this equation, the dimensionless constant C is determined by the geometry of the lattice and takes the value -1.444 for a bcc structure. The negative sign signifies that the electrostatic potential energy in the lattice corresponds to a binding interaction. The quantities e^2 , n_e , and Z correspond, respectively, to the strength of the Coulomb

interaction between charged particles, the density of the electron number which, in fully ionized matter, is directly related to the density of positive ions as a result of charge neutrality and the atomic number of the element.

The second term on the right hand side of equation (23) represents the relativistic dispersion relation integrand of the electrons, originating from the distribution of electron momenta k up to Fermi momentum k_F , which determines the highest occupied momentum state at zero temperature, respectively. The symbol m_e denotes the electron rest mass, incorporating relativistic effects into the pressure calculation, which is an essential aspect for accurately modeling high density environments. The factor $1/(3\pi^2 h^3)$ arises from the proper normalization of the three dimensional momentum space volume, where h denotes Planck's constant. This coefficient guarantees that the integral over the distribution of electron momenta is dimensionally consistent and accurately scaled. When combined, these components yield the EoS for WD matter in the absence of magnetic fields, accounting for the influence of electron degeneracy and the structural role of the ionic lattice.

Following [77], we assume that the total energy density $\rho_{\text{crust}}(k_F)$ in the matter located in the crust of the strange dwarf which includes the contributions from nuclei, electrons, and the ionic lattice is expressed as

$$\begin{aligned} \rho_{\text{crust}}(k_F) &= \rho_L + \rho_e + \rho_i - \rho_\epsilon, \\ &= C e^2 n_e^{4/3} Z^{2/3} + \frac{1}{\pi^2 h^3} \int_0^{k_F} \sqrt{k^2 + m_e^2} k^2 dk \\ &\quad + n_i M(Z, A) - n_e m_e. \end{aligned} \quad (25)$$

As can be seen, the total energy density is composed of several distinct contributions. The first component, ρ_L , accounts for the energy density associated with the Coulomb lattice formed by the ions. The second, ρ_e , corresponds to the energy density of the degenerate electron gas, which includes the relativistic energy of electrons integrated from zero momentum up to the Fermi momentum. The third term, ρ_i , refers to the rest mass energy density of fully ionized atomic nuclei, where n_i denotes the ion number density and $M(Z, A)$ is the nuclear mass of an ion with atomic number Z and mass number A . The fourth contribution, ρ_ϵ , serves as a correction by subtracting the electron rest mass energy that is already implicitly included in the nuclear mass $M(Z, A)$, thereby preventing the electron rest energy from being counted twice in the total. Taken together, these components form a self-consistent and physically complete expression for the crust energy density of SD matter under the assumptions of full degeneracy, absence of magnetic fields, and a crystallized plasma structure. In our study, we adopt carbon as the elemental composition of the crust material, setting $Z = 6$ and $A = 12$, which corresponds to fully ionized ^{12}C . The nuclear mass $M(6, 12)$ used in the calculations is taken from experimental atomic mass evaluations, ensuring alignment with the most up-to-date empirical measurements [74, 75].

Following the classical approach in [39, 87], we there-

fore assume a pure carbon composition for the hadronic crust of the SD models. This choice provides both physical consistency and observational relevance, since most well studied WDs exhibit outer layers dominated by C/O mixtures. From a structural perspective, adopting heavier compositions such as O/Ne/Mg only shifts the mass radius curve slightly toward smaller radii, by less than $\sim 3\%$ in both M and R , as shown in relativistic calculations for massive WDs [89]. Such deviations lie well within the current observational uncertainties [88], and therefore do not affect the global trend that rotating SDs remain observationally indistinguishable from ordinary WDs. Preliminary calculations with O/Ne/Mg crusts confirm that this indistinguishability persists within the expected precision of future *Gaia* and LISA observations. Hence, the adoption of a carbon crust represents a consistent and conservative approximation for the present investigation.

3.2. Core Matter Composition

For the EoS employed in the core of the SD, we adopt one that describes quark matter with a self-bound phase composed of deconfined u , d , and s quarks. In this framework, matter is assumed to be a zero temperature Fermi gas consisting of massless u , d , and s quarks, enclosed by the QCD vacuum energy density, commonly referred to as the bag constant \mathcal{B} . Modifications arising from gluonic dynamics and color-superconducting pairing effects are omitted in this treatment, given that their influence on the structure of low mass configurations is expected to be minimal, typically below the 1% level [90]. Consequently, the resulting EoS takes the form:

$$p_{\text{core}} = \frac{\rho_{\text{core}} - 4\mathcal{B}}{3}, \quad (26)$$

with ρ_{core} being the energy density of the quark. In line with the classical framework of [91] and the phenomenological calibration of [92], we employ a bag constant of $\mathcal{B}^{1/4} = \{135, 145, 160\} \text{ MeV}$. Following common practice, we quote the bag parameter through $B^{1/4}$ (in MeV) and convert it to B in MeV fm^{-3} using $B = (B^{1/4})^4/(\hbar c)^3$. This choice ensures an energy per baryon in the range $\rho_{\text{core}}/A = 875\text{--}894 \text{ MeV}$, remaining well beneath the stability threshold set by iron at 930.4 MeV, thereby satisfying the absolute stability condition for SQM.

4. RESULTS

4.1. Sensitivity of the hybrid EoS to the bag constant

Throughout this section, we adopt the cold limit ($T = 0$), which is well justified for compact objects older than $\gtrsim 10^8 \text{ yr}$, for which thermal contributions to the pressure are negligible compared to electron degeneracy. In

addition, SDs may retain residual magnetic fields inherited from their WD progenitors, typically in the range $10^3\text{--}10^5 \text{ G}$ [94]. Such fields are dynamically irrelevant for global hydrostatic equilibrium: they do not significantly modify the mass radius relation, especially compared to the few percent variations induced by the bag constant scan summarized in Table I and quantified by $\Delta M_{\text{max}}(\mathcal{B})$ in Eq. (27).

However, magnetically induced anisotropies can affect percent level features of the crustal structure and the directional components of the stress tensor, as shown by [93]. Although these effects remain subdominant in the context of equilibrium modeling, they may become relevant for oscillation spectra or multipolar deformations and thus may provide complementary diagnostics in future studies. A fully magnetostatic treatment, incorporating magnetic-field-dependent corrections to the EoS and anisotropic pressure contributions, will be addressed in a forthcoming work.

To see the sensibility of the EoS with the change of the bag constant in the quark-matter sector, we considered three representative values of the bag constant ($\mathcal{B}^{1/4} = \{135, 145, 160\} \text{ MeV}$), while keeping all other microphysics and the crustal composition fixed (pure ^{12}C ; same electrostatic matching and transition criterion). For each \mathcal{B} considered, we construct the hybrid EoS and compute the corresponding sequence $M - R$ by integrating the TOV equations.

Figure 1 shows the fluid pressure versus energy density profile for three different bag constants, highlighting the abrupt transition between the crust dominated by electron degeneracy pressure and the core, composed of quark matter. This discontinuity provides the microscopic foundation for the macroscopic stellar sequences discussed below. At low and intermediate densities, $\rho \lesssim \rho_{\text{drip}}$, the curves coincide because they are independent of the description of the quark matter. However, above the neutron-drip density, where the SQM core begins to play a significant role, smaller values of (\mathcal{B}) lead to higher fluid pressure at a fixed energy density, whereas larger values of (\mathcal{B}) result in lower fluid pressure. This behavior is fully consistent with the standard MIT bag-model phenomenology.

Once the EoS is defined, we solve the TOV equations to analyze the equilibrium of non-rotating stars for different values of \mathcal{B} . In this way, the effects of the bag constant on the mass, normalized in solar masses, as a function of the radius are shown in Fig. 2 considering three different values of \mathcal{B} . The overall shape of the $M - R$ curves is essentially preserved across the range of the bag constant considered. For each value of \mathcal{B} , we compute the maximum mass M_{max} , the corresponding radius $R(M_{\text{max}})$, and the central density $\rho_c(M_{\text{max}})$; see Table I. To make the comparison explicit, we define the relative variation of the maximum mass with respect to the reference value $\mathcal{B}_{\text{ref}}^{1/4} = 145 \text{ MeV}$,

$$\Delta M_{\text{max}}(\mathcal{B}) = \frac{M_{\text{max}}(\mathcal{B}) - M_{\text{max}}(\mathcal{B}_{\text{ref}})}{M_{\text{max}}(\mathcal{B}_{\text{ref}})} \times 100\%, \quad (27)$$

TABLE I: Sensitivity of the maximum mass with the bag constant. For each value of \mathcal{B} , the maximum mass M_{\max} , the corresponding radius $R(M_{\max})$ and central density $\rho_c(M_{\max})$, and the relative variation $\Delta M_{\max}(\mathcal{B})$ with respect to the reference value $\mathcal{B}_{\text{ref}}^{1/4} = 145$ MeV are indicated.

$\mathcal{B}^{1/4}$ [MeV]	M_{\max} [M_{\odot}]	$R(M_{\max})$ [km]	$\rho_c(M_{\max})$ [10^6 g cm^{-3}]	ΔM_{\max} [%]
134	1.3596	447.15	173.234	-0.0370
145	1.3601	452.02	230.61	0.0000
160	1.3608	452.91	341.98	+0.0520

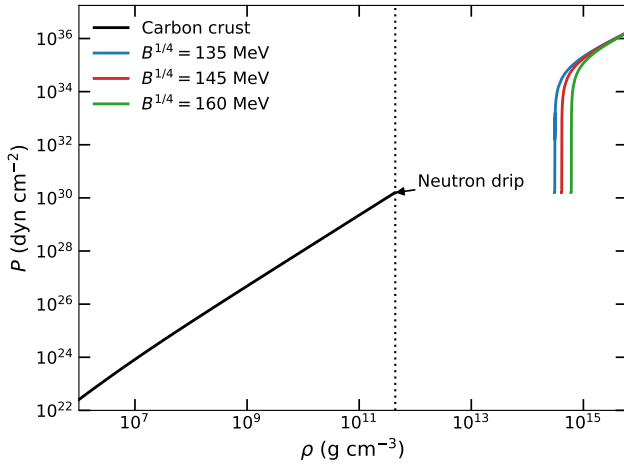


FIG. 1: Fluid pressure against the energy density (carbon crust + SQM core) for $\mathcal{B}^{1/4} = \{135, 145, 160\}$ MeV. Differences appear only above neutron-drip density, where the SQM core starts to play a significant role. These trends explain the small shifts observed in the M - R curves in Fig. 2.

which remains at the level of only a few percent over the explored range. This analysis shows that reasonable variations of the bag constant produce M - R curves that are nearly indistinguishable within current and near future measurement uncertainties.

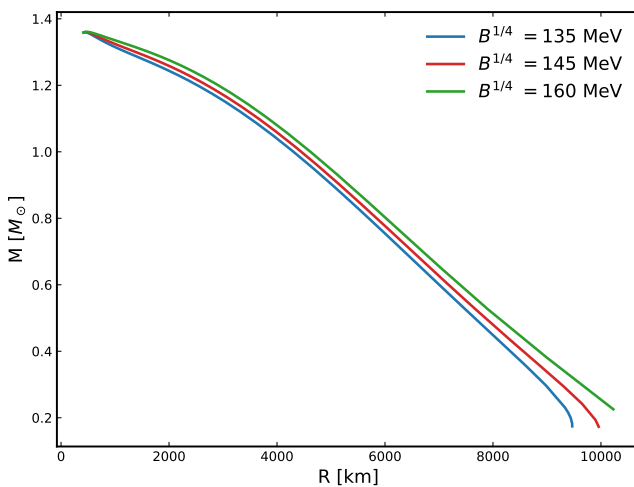


FIG. 2: Mass-radius relations for SDs computed with $\mathcal{B}^{1/4} = \{135, 145, 160\}$ MeV.

4.2. Effects of the rotation on SDs

The static background is obtained by integrating Eqs. (4)–(6) with a standard adaptive Runge–Kutta scheme, and the Hartle–Thorne perturbation equations are then integrated on top of the same background. To anticipate common referee concerns, a minimal robustness check consists of recomputing representative models while tightening/loosening the integrator tolerances and varying the matching tolerance at the core–crust interface, and verifying that the reported global quantities (M, R, J) and the locations of qualitative features (e.g., the onset of the core and the approach to the WD branch) remain unchanged within plotting resolution. A compact summary of these checks can be reported in a short appendix, without modifying the main analysis.

The equilibrium properties of SDs were computed by solving the TOV equations for the static case and then extended for rotating configurations using the Hartle–Thorne slow rotation formalism. The adopted EoS, which depicts a crystalline carbon crust and a SQM core described by the MIT Bag Model, naturally introduces a density discontinuity at the core–crust interface. This discontinuity is a key feature that distinguishes SDs from ordinary WDs.

For the static sequences, we restrict attention to the usual stable branch selected by the turning-point condition along the one-parameter family of equilibria, $dM/d\rho_c > 0$ (equivalently, before the first maximum of $M(\rho_c)$), which is a standard necessary criterion for radial stability of cold compact stars. For hybrid configurations with a sharp interface, full dynamical stability can depend on the assumed boundary conditions and phase-conversion rate at the interface; we therefore interpret $dM/d\rho_c > 0$ as a practical screening criterion and refer the reader to [6, 7, 11] for detailed treatments of radial modes in the presence of a density discontinuity. For rotating models within the Hartle–Thorne approximation, the same turning-point logic provides a useful guide, but configurations near $\Omega \sim \Omega_K$ should be assessed with fully two-dimensional methods.

Having established the microscopic foundation through the EoS, we now turn to the macroscopic implications of stellar rotation, particularly the role of the Keplerian limit in determining the equilibrium configuration and observable properties of SDs. Figure 3 presents the energy density and mass profiles as functions of the radial coordinate and total radius in the top and bottom panels, respectively, for a static WD, a static SD, and uniformly

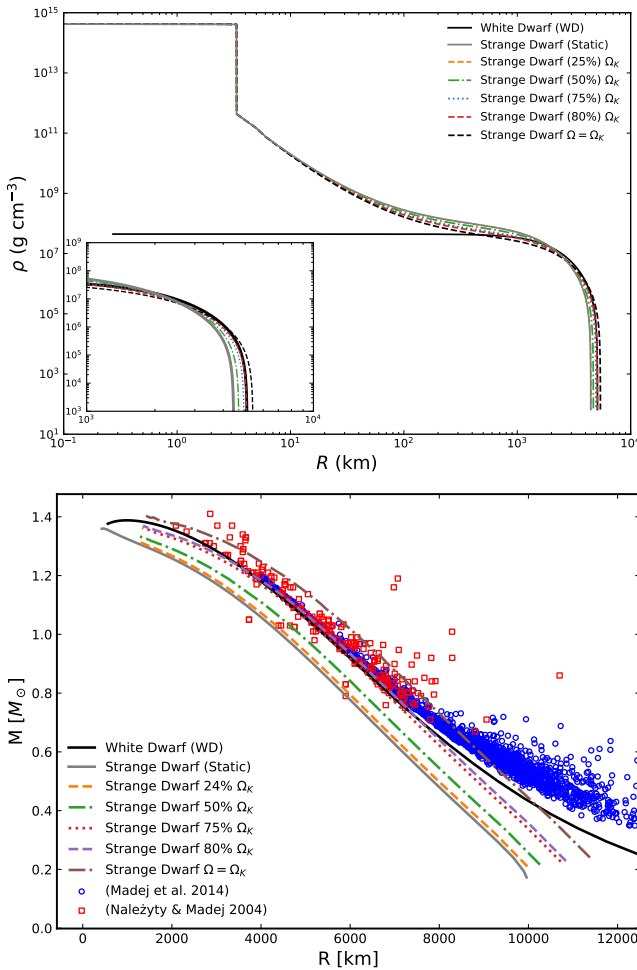


FIG. 3: Top: Radial energy-density profiles for a $1 M_{\odot}$ configuration. The SD profile shows an extended near-constant-density quark core and an abrupt density jump at the core–crust interface (at fixed pressure), whereas the WD profile is smooth. Bottom: M – R relations for a pure carbon crust and a quark-matter core, compared with observational data (blue circles from [96] and red squares from [95]). The key takeaway is that increasing rotation inflates the SD radius and drives the rotating SD sequences toward the WD locus in the (M, R) plane, motivating a quantitative “indistinguishability” criterion discussed in the main text.

rotating SDs at various fractions of the Keplerian frequency Ω_K . In the top panel, the static WD exhibits an energy density that remains nearly constant with increasing radius until it approaches the stellar surface, where it then decreases monotonically. In contrast, the SD maintains an almost uniform energy density throughout its quark matter core. At the core envelope interface, the density drops abruptly at fixed fluid pressure, after which it decreases monotonically with radius through the crystalline envelope. In the bottom panel, the impact of rotation is clearly visible. These theoretical results are shown alongside observational data extracted from the catalogs listed in [96] and [95], plotted as blue circles and red squares, respectively.

As the rotation rate increases, the stellar radius of an

SD grows and approaches the characteristic radius of a WD. This comparison suggests that compact objects containing quark matter may be observationally misclassified as WDs, given that measurements are typically limited to global quantities such as mass and radius, highlighting the urgent need for observational diagnostics capable of probing their innermost composition. Therefore, complementary diagnostics such as tidal deformability or continuous gravitational wave emission may be essential for unambiguously identifying rotating SDs [5, 8].

In addition, because the mass radius curves exhibit very little sensitivity to reasonable variations in the quark matter sector as discussed in Subsection 4.1 and illustrated in Figs. 1 and 2 varying the bag constant within the range $\mathcal{B}^{1/4} = 135, 145, 160$ MeV modifies the maximum mass and corresponding radius by only a few percent (see, also, Table I). Thus, the overall morphology of the M – R curves, as well as their overlap with the WD domain, remains essentially unchanged. Thus, the observational indistinguishability between rotating SDs and massive WDs does not depend on a finely tuned choice of the bag constant.

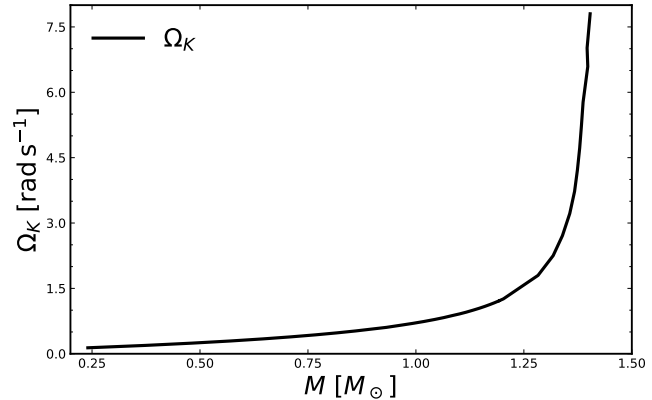


FIG. 4: Kepler (mass-shedding) angular frequency $\Omega_K(M)$ for the SD sequences, shown here as a reference spin scale. Within the Hartle–Thorne approach, Ω_K is used to normalize the rotation rate; statements very near $\Omega \sim \Omega_K$ should be interpreted conservatively given the slow-rotation truncation.

5. CONCLUSION

The present investigation analyzes how the presence of a quark matter core would imprint itself on the global properties of compact stars that, at first glance, resemble ordinary WDs. The stellar fluid is modeled with a crust composed of a degenerate electron gas and a core of quark matter. By solving the TOV equations in conjunction with the Hartle–Thorne general relativistic formalism with uniform rotation, we construct sequences of SDs ranging from the non-rotating limit up to their individual Kepler frequencies, where the mass shedding occurs.

For this model, three fundamental conclusions can be

drawn. (1) The associated decrease in central density implies that, for $R \gtrsim 10^3$ km, the pressure gradient is dominated by the electron gas, while the quark-matter core although still present becomes hydrostatically negligible; since, using this model, radii similar to those of white dwarfs are found. This convergence is illustrated by the radial energy density profiles shown in Fig. 3. (2) Rotation affects the SD mass radius sequence: as the fractional spin Ω/Ω_K increases from 0 to 1, the radius of a given mass increases until the rotating SD branch converges with the WD curve. Consequently, a SD spinning at $\gtrsim 75\%$ of Ω_K becomes practically indistinguishable from a WD in the M - R plane. (3) The computed Keplerian curve, $\Omega_K(M)$, defines a strict centrifugal limit. Nevertheless, for any given mass, there exists a broad sub Keplerian range in which the mass of an SD can coincide with that of a WD, rendering the two classes observationally indistinguishable when only global parameters such as mass or radius are considered.

The results reported in this article corroborate and significantly extend the seminal conjecture of Alcock, Farhi, and Olinto (1986) that SQM cores may reside within stars exhibiting WD-like radii. In contrast to Chandrasekhar's classical 1939 mass limit [63], our models show that incorporating rapid rotation and a deconfined quark-matter core increases the effective upper mass of WD-like objects by $\gtrsim 10\%$ at the Keplerian threshold Ω_K , while preserving the canonical limit $\leq 1.4 M_\odot$ for slowly rotating configurations. By employing the Hartle–Thorne formalism within full general relativity rather than relying on a Newtonian centrifugal correction this work extends the pioneering analysis of uniformly rotating dwarfs by Hartle and Thorne (1968) [82]. Given that Hartle–Thorne is a slow rotation expansion, our results are best interpreted as capturing robust leading-order rotational trends and delineating where SD/WD degeneracy emerges, while the immediate vicinity of mass shedding should be revisited with fully two-dimensional relativistic rotating-star calculations.

Crucially, our results indicate that global observables alone such as mass, radius, luminosity, or spin period are insufficient to reveal the presence of quark matter when $\Omega/\Omega_K \lesssim 0.8$. This constrains the parameter space

in which alternative diagnostics (e.g., asteroseismology, gravitational redshift spectroscopy, or tidal deformability measurements from inspiral events) must be pursued.

It is worth highlighting that the adoption of a carbon crust in the hybrid EoS does not constitute a restrictive assumption. Theoretical estimates show that heavier crusts (O/Ne/Mg) would modify the stellar mass and radius by less than $\sim 3\%$ [89], a level well below the precision of current mass-radius measurements [88]. Consequently, the main conclusion of this work that rotation obscures the presence of a quark core in SDs remains robust against plausible variations in crustal composition. In addition to the crustal composition, we have explicitly tested the dependence of our results on the quark-matter sector by performing a bag constant sensitivity analysis over the range of \mathcal{B} . As shown in Sec. 3 and summarized in Table I, the resulting variations in the maximum mass, corresponding radius, and central density remain at the level of only a few percent, preserving the overall morphology of the M - R curves. This demonstrates that rapid rotation can effectively mask the presence of a quark core in SDs.

Finally, this study contributes new nuance to ongoing debates concerning the astrophysical census of compact objects. Because sub Keplerian SDs occupy the same region of the M - R diagram as WDs, a non-negligible fraction of the current WD catalog classified based on photometry and parallax may, in fact, contain hybrid stars. Our sequences provide concrete diagnostic criteria, particularly deviations in the quadrupole moment or in the low- ℓ g -mode spectra, which could distinguish between the two populations in future high precision surveys.

Acknowledgments

EO acknowledges support from FUNCAP(BP6-0241-00335.01.00/25). JDVA thanks Universidad Privada del Norte and Universidad Nacional Mayor de San Marcos for the financial support - RR N°005753-2021-R/UNMSM under the project number B21131781.

[1] I. Caiazzo et al., *Nature* **595**, 39 (2021).
[2] M. Kilic et al., *Mon. Not. R. Astron. Soc.* **522**, 2181 (2023).
[3] P. Bergeron et al., *Astrophys. J.* **876**, 67 (2019).
[4] C. Alcock, and A. Olinto, *Annu. Rev. Nucl. Part. Sci.* **38**, 161 (1988).
[5] N. K. Glendenning, Ch. Kettnet and F. Weber, *Phys. Rev. Lett.* **74**, 3519 (1995).
[6] J. P. Pereira, C. V. Flores and G. Lugones, *Astrophys. J.* **860**, 12 (2018).
[7] F. Di Clemente, M. Mannarelli and F. Tonelli, *Phys. Rev. D* **101**, 103003 (2020).
[8] L. Perot, N. Chamel and P. Vallet, *Phys. Rev. D* **107**, 103004 (2023).
[9] A. Kurban, Y. Huang, J. Geng and H. Zong, *Phys. Lett. B* **832**, 137204 (2022).
[10] K. Wang et al., *Astrophys. J.* **936**, 5 (2022).
[11] M. G. Alford, S. P. Harris and P. S. Sachdeva, *Astrophys. J.* **847**, 109 (2017).
[12] F. Di Clemente, A. Drago, P. Char and G. Pagliara, *Astron. Astrophys.* **678**, L1 (2023).
[13] F. Di Clemente, A. Drago and G. Pagliara, *Universe* **10**, 322 (2024).
[14] K. Boshkayev, J. A. Rueda, R. Ruffini and I. Siutsou, *Astrophys. J.* **762**, 117 (2013).
[15] L. Becerra, K. Boshkayev, J. A. Rueda and R. Ruffini, *Mon. Not. R. Astron. Soc.* **487**, 812 (2019).
[16] M. F. Souza, J. G. Coelho and J. C. N. de Araújo, *Mon.*

Not. R. Astron. Soc. **492**, 5949 (2020).

[17] R. Di Stefano, R. Voss, and J. S. W. Claeys, *Astrophys. J.* **738**, L1 (2011).

[18] G. O. da Rosa, S. O. Kepler, L. T. T. Soethe, A. D. Romero and K. J. Bell, *Astrophys. J.* **974**, 314 (2024).

[19] Alcock, C., Farhi, E., & Olinto, A. (1986). Strange stars. *Astrophysical Journal, Part 1* (ISSN 0004-637X), vol. 310, Nov. 1, 1986, p. 261-272., 310, 261-272.

[20] E. Witten, “Cosmic separation of phases”, *Phys. Rev. D* **30**, 272 (1984).

[21] Bodmer, A. R. (1971). Collapsed nuclei. *Physical Review D*, 4(6), 1601.

[22] Baym, G., Pethick, C., & Sutherland, P. (1971). The ground state of matter at high densities: equation of state and stellar models. *Astrophysical Journal*, vol. 170, p. 299, 170, 299.

[23] R. C. Tolman, “Static solution of Einstein’s field equation for spheres of fluid”, *Phys. Rev. D* **55**, 364 (1939).

[24] J. R. Oppenheimer and G. Volkoff, “On massive neutron cores”, *Phys. Rev. D* **55**, 374 (1939).

[25] Glendenning, N. K. (2012). *Compact stars: Nuclear physics, particle physics and general relativity*. Springer Science & Business Media.

[26] Johnson, K. (1975). The MIT bag model. *Acta Phys. Pol. B*, 6(12), 8.

[27] Chodos, A. J. R. L., Jaffe, R. L., Johnson, K., Thorn, C. B., & Weisskopf, V. (1974). New extended model of hadrons. *Physical Review D*, 9(12), 3471.

[28] Broadhurst, D. J. (1976). Current algebra of quarks confined to a cavity. *Nuclear Physics B*, 105(2), 319-332.

[29] K. Chakraborty, F. Rahaman, and A. Mallick, “A relativistic two-fluid model of compact stars”, *Modern Physics Letters A* **32**, 1750055 (2017).

[30] E. Farhi and R. L. Jaffe, “Strange matter”, *Phys. Rev. D* **30**, 2379 (1984).

[31] Haensel, P., Zdunik, J. L., & Schaefer, R. (1986). Strange quark stars. *Astronomy and Astrophysics* (ISSN 0004-6361), vol. 160, no. 1, May 1986, p. 121-128., 160, 121-128.

[32] R. F. Tooper, “Adiabatic Fluid Spheres in General Relativity”, *Astrophys. J.* **142**, 1541 (1965).

[33] Arbañil, J. D., Lemos, J. P., & Zanchin, V. T. (2013). Polytropic spheres with electric charge: compact stars, the Oppenheimer-Volkoff and Buchdahl limits, and quasiblack holes. *Physical Review D*, 88(8), 084023.

[34] Glendenning. Nuclear solid crust on rotating strange quark stars.

[35] S. Han and A. W. Steiner. “Tidal deformability with sharp phase transitions in binary neutron stars”, *Phys. Rev. D* **99**, 083014 (2019); arXiv:1810.10967 [nucl-th].

[36] M. G. Alford, S. P. Harris, and P. S. Sachdeva, “On the Stability of Strange Dwarf Hybrid Stars”, *Astrophys. J.* **847**, 109 (2017).

[37] J. D. V. Arbañil and M. Malheiro, “Radial stability of anisotropic strange quark stars”, *J. Cosmol. Astropart. Phys.* 11, (2016) 012; arXiv:1607.03984 [astro-ph.HE].

[38] J. P. Pereira, C. Vásquez-Flores and G. Lugones, “Phase transition effects on the dynamical of hybrid neutron stars”, *Astrophys. J.* **860**, 1 (2018); arXiv:1706.09371 [gr-qc].

[39] N. K. Glendenning, Ch. Kettner, and F. Weber, “From Strange Stars to Strange Dwarfs”, *Astrophys. J.* **450**, 253 (1995).

[40] G. Lugones and A. G. Grunfeld, “Phase Conversions in Neutron Stars: Implications for Stellar Stability and Gravitational Wave Astrophysics”, *Universe* **2021**, 7, 493.

[41] F. Di Clemente, A. Drago, P. Char, and G. Pagliara, “Stability and instability of strange dwarfs”, arXiv:2207.08704v1 [astro-ph.SR].

[42] G. Lugones, M. Mariania, and I. F. Ranea-Sandoval, “A model-agnostic analysis of hybrid stars with reactive interfaces”, *J. Cosmol. Astropart. Phys.* 03, (2023) 028.

[43] M. B. Albino, F. S. Navarra, R. Fariello, and G. Lugones, “The nature of the quark-hadron phase transition in hybrid stars and the mass-radius diagram”, *J. Phys. Conf. Ser.* **2340**, 012015 (2022).

[44] ANNALA, Eemeli, et al. Evidence for quark-matter cores in massive neutron stars. *Nature Physics*, 2020, vol. 16, no 9, p. 907-910.

[45] J. D. V. Arbañil, L. S. Rodrigues, and C. H. Lenzi, “Phase transition and stiffer core fluid in neutron stars: effects on stellar configurations, dynamical stability, and tidal deformability”, *Eur. Phys. J. C* **83**, 211 (2023).

[46] S. L. Shapiro and S. A. Teukolsky, *Black holes, white dwarfs, and neutron stars: The physics of compact objects* (Wiley, New York, 1983).

[47] B. P. Abbott et al., “Observation of gravitational waves from binary black hole merger”, *Phys. Rev. Lett.* **116**, 061102 (2016); arXiv:1602.03837 [gr-qc].

[48] B. P. Abbott et al., “GW151226: Observation of Gravitational Waves from a 22-Solar-Mass Binary Black Hole Coalescence”, *Phys. Rev. Lett.* **116**, 241103 (2016); arXiv:1606.04855 [gr-qc].

[49] B. P. Abbott et al., “GW170817: Observation of gravitational waves from a Binary Neutron Star Inspiral”, *Phys. Rev. Lett.* **119**, 161101 (2017); arXiv:1710.05832 [gr-qc].

[50] B. P. Abbott et al., “GW170104: Observation of a 50-Solar-Mass Binary Black Hole Coalescence at Redshift 0.2”, *Phys. Rev. Lett.* **118**, 221101 (2017); arXiv:1706.01812 [gr-qc].

[51] B. P. Abbott et al., “GW170814: A Three-Detector Observation of Gravitational Waves from a Binary Black Hole Coalescence”, *Phys. Rev. Lett.* **119**, 141101 (2017); arXiv:1709.09660 [gr-qc].

[52] B. P. Abbott et al., “GW170608: Observation of a 19 Solar-mass Binary Black Hole Coalescence”, *Astrophys. J. Lett.* **851**, L35 (2017); arXiv:1711.05578 [astro-ph.HE].

[53] B. P. Abbott et al., “Astrophysical implications of the binary black hole merger GW150914”, *Astrophys. J. Lett.* **818**, L22 (2016); arXiv:1602.03846 [astro-ph.HE].

[54] B. P. Abbott et al., “Tests of General Relativity with GW150914”, *Phys. Rev. Lett.* **116**, 221101 (2016). Erratum: “Tests of General Relativity with GW150914 [Phys. Rev. Lett. 116, 221101 (2016)]”, *Phys. Rev. Lett.* **121**, 129902(E) (2018); arXiv:1602.03841 [gr-qc].

[55] B. P. Abbott et al., “Multi-messenger observational of a binary neutron star merger”, *Astrophys. J. Lett.* **848**, L12 (2017); arXiv:1710.05833 [astro-ph.HE].

[56] M. G. Orsaria, G. Malfatti, M. Mariani, I. F. Ranea-Sandoval, F. García, W. M. Spinella, G. A. Contrera, G. Lugones, and F. Weber, “Phase transition in neutron stars and their links to gravitational waves”, *J. Phys. G: Nucl. Part. Phys.* **46**, (2019) 073002.

[57] L. Tonetto and G. Lugones, “Discontinuity gravity modes in hybrid stars: Assessing the role of rapid and slow phase conversions”, *Phys. Rev. D* **101**, 123029 (2020).

[58] V. K. Gupta, V. Tuli, and A. Goyal, “Radial Oscillations of Hybrid Stars”, *Astrophys. J.* **579**, 374 (2002);

arXiv:astro-ph/0202016.

[59] C. Vásquez-Flores, C. H. Lenzi, and G. Lugones, “Radial pulsations of hybrid neutron stars”, *Int. J. Modern Physics Conf. Ser.* **18**, 105 (2012).

[60] M. Mariani, M. G. Orsaria, I. F. Ranea-Sandoval, G. Lugones, “Magnetized hybrid stars: effects of slow and rapid phase transitions at the quark–hadron interface”, *Mon. Not. R. Astron. Soc.* **489**, 4261 (2019); arXiv:1909.08661 [astro-ph.HE].

[61] P. Haensel, J. L. Zdunik, and R. Schaeffer, “Phase transition in dense matter and radial pulsation of neutron stars”, *Astron. Astrophys.* **217**, 137 (1989).

[62] J. D. V. Arbañil, J. P. S. Lemos, and V. T. Zanchin, “Polytropic spheres with electric charge: compact stars, the Oppenheimer-Volkoff and Buchdahl limits, and quasiblack holes”, *Phys. Rev. D* **88**, 084023 (2013); arXiv:1309.4470 [gr-qc].

[63] S. Chandrasekhar, “An Introduction to the Study of Stellar Structure (Chicago University Press, 1939) p.52.

[64] J. P. Pereira, J. G. Coelho, and J. A. Rueda, “Stability of thin-shell interfaces inside compact stars”, *Phys. Rev. D* **90**, 123011 (2014); arXiv:1412.1848 [gr-qc].

[65] J. P. Pereira and J. A. Rueda, “Radial stability in stratified stars”, *Astrophys. J.* **801**, 1 (2015); arXiv:1501.02621 [gr-qc].

[66] H. A. Buchdahl, “General relativistic fluid spheres”, *Phys. Rev.* **116**, 1027 (1959).

[67] C. W. Misner and H. S. Zapsolsky, “High-density behavior and dynamical stability of neutron star models”, *Phys. Rev. Lett.* **13**, 122 (1964).

[68] P. Haensel, A. Y. Potekhin, and D. G. Yakovlev *Neutron Stars 1: Equation of State and Structure* (Springer Verlag, New York, 2007).

[69] R. F. Tooper, “General relativistic polytropic fluid spheres”, *Astrophys. J.* **140**, 434 (1964).

[70] H. Sotani, N. Yasutake, T. Maruyama and T. Tatsumi, “Density discontinuity of a neutron star and gravitational waves”, *Phys. Rev. D* **65**, 024010 (2001).

[71] Salpeter, E. E. 1961, *Astrophys. J.* , 134, 669

[72] Hamada, T., & Salpeter, E. E. 1961, *Astrophys. J.* , 134, 683

[73] Otoniel, E., Franzon, B., Carvalho, G. A., Malheiro, M., Schramm, S., & Weber, F. 2019, *Astrophys. J.* , 879, 46. doi:10.3847/1538-4357/ab24d1

[74] Wang, M., Audi, G., Wapstra, A. H., Kondev, F. G., MacCormick, M., Xu, X., & Pfeiffer, B. 2012, *Chinese Physics C*, 36, 1603

[75] Audi, G., Wang, M., Wapstra, A. H., Kondev, F. G., MacCormick, M., Xu, X., & Pfeiffer, B. 2012, *Chinese Physics C*, 36, 1287

[76] Shapiro, S. L., & Teukolsky, S. A. 2008, *Black Holes, White Dwarfs, and Neutron Stars: The Physics of Compact Objects* (Weinheim: John Wiley & Sons)

[77] Chamel, N., Fantina, A. F., & Davis, P. J. 2013, *Phys. Rev. D* , 88, 081301(R)

[78] Gamow, G. 1939, *Physical Review*, 55, 718–725

[79] Chamel, N., Molter, E., Fantina, A. F., & Arteaga, D. P. 2014, *Phys. Rev. D* , 90, 043002

[80] Chamel, N., & Fantina, A. F. 2015, *Phys. Rev. D* , 92, 023008

[81] Hartle, J. B., 1967, *Astrophys. J.* , 150, 1005.

[82] Hartle, J. B. and Thorne K. S., 1968, *Astrophys. J.* , 153, 807.

[83] Glendenning, N. K. and Weber, F. (1994). Impact of frame dragging on the Kepler frequency of relativistic stars, *Physical Review D*, 50, pp. 3836-3841.

[84] Weber, F. and Glendenning, N. K. (2012). Application of the improved Hartle method for the construction of general relativistic rotating neutron star models, *The Astrophysical Journal*, 390, pp. 541.

[85] Weber, F. and Glendenning, N. K. and Weigel, M. K. (1991). Structure and stability of rotating relativistic neutron stars, *The Astrophysical Journal*, 373, pp. 579.

[86] Friedman, J. L. and Ipser, J. R. and Parker, L. (1986) Rapidly rotating neutron star models, *The Astrophysical Journal*, 304, pp. 115-139

[87] O. G. Benvenuto and L. G. Althaus, “The Structure and Thermal Evolution of Strange Dwarf Stars,” *The Astrophysical Journal*, vol. 462, p. 364, May 1996. doi: 10.1086/177158.

[88] G. J. Mathews, I.-S. Suh, B. O’Gorman, N. Q. Lan, W. Zech, K. Otsuki, and F. Weber, “Analysis of white dwarfs with strange-matter cores,” *Journal of Physics G: Nuclear and Particle Physics*, vol. 32, no. 6, pp. 747–759, Jun. 2006. doi: 10.1088/0954-3899/32/6/001.

[89] M. Malheiro, E. Otoniel, and J. G. Coelho, “Relevance of Dynamical Nuclear Processes in Quantum Complex Systems of Massive White Dwarfs,” *Brazilian Journal of Physics*, vol. 51, no. 2, pp. 223–230, Apr. 2021. doi: 10.1007/s13538-020-00840-0.

[90] M. Alford, K. Rajagopal and F. Wilczek, “Color-flavor locking and chiral symmetry breaking in high density QCD,” *Nucl. Phys. B* **537**, 443 (1999).

[91] C. Alcock, E. Farhi and A. Olinto, “Strange stars,” *Astrophys. J.* **310**, 261 (1986).

[92] E. Farhi and R. L. Jaffe, “Strange matter,” *Phys. Rev. D* **30**, 2379 (1984).

[93] D. Rodríguez Concepción and J. Quintero Angulo, “Model dependence of the magnetic-field effects on compact stars,” *Phys. Rev. D* **107**, 083008 (2023).

[94] D. Bagdasaryan, “Magnetic field of strange dwarfs,” *Astrophysics* **59**, 241–248 (2016).

[95] Należyty, M., & Madej, J. 2004, *Astronomy & Astrophysics*, 420, 507

[96] Madej, J., Należyty, M., & Althaus, L. G. 2004, *Astronomy & Astrophysics*, 419, L5